ELSEVIER

Journal of Molecular Catalysis A: Chemical 132 (1998) 241–253

JOURNAL OF MOLECULAR CATALYSIS A: CHEMICAL

Synthesis, characterization and catalytic properties of bimetallic $ZrMo_2N_x$–Mo_2N nitrides of high surface area

Y. Zhang [a], Y. Li [b,c,*], R. Raval [b,c], C. Li [a], R. Zhai [a], Q. Xin [a]

[a] *State Key Laboratory of Catalysis, Dalian Institute of Chemical Physics, Chinese Academy of Sciences, Dalian 116023, China*
[b] *Leverhulme Centre for Innovative Catalysis, Chemistry Department, Liverpool University, Liverpool L69 3BX, UK*
[c] *Interdisciplinary Research Centre in Surface Science, Chemistry Department, Liverpool University, Liverpool L69 3BX, UK*

Received 15 April 1997; accepted 16 October 1997

Abstract

A set of bimetallic nitrides, $ZrMo_2N_x$–Mo_2N, of high specific surface area up to 132 m^2/g has been synthesized by temperature programmed nitriding (TPN) mixtures of Zr- and Mo-containing compounds with ammonia. Two series of precursors have been studied using XRD, SEM and FT-IR. It is found that the structure and composition of the end-products depend on the properties of the precursors and these, in turn, are influenced to a large extent by the preparation method of the precursor, i.e. using impregnation or using coprecipitation. The end-catalysts obtained from precursors prepared by impregnation are composed of ZrO_2–Mo_2N while those from precursors prepared by coprecipitation consist of $ZrMo_2N_x$–Mo_2N. XRD and SEM results reveal that the characteristic platelet structure of MoO_3 is damaged upon the introduction of the second metal component by coprecipitation, but is retained when using impregnation. The catalytic activities of the bimetallic nitrides for the hydrogenation of cyclohexene and the hydrodesulfurization of thiophene are found, under medium pressures (3.0 MPa), to compare favourably with those of a commercial sulfided $NiCoMo/Al_2O_3$ catalyst and unsupported γ-Mo_2N. H_2-TPD results indicate that the bimetallic nitrides possess a more extensive capacity for hydrogen adsorption in low temperature states.

Keywords: Nitride; Bimetallic; Catalysis; Molybdenum; Zirconium; XRD; SEM; FTIR; HDS; TPD; DTA; Topotactic; Impregnation; Coprecipitation; MoO_3; Mo_2N

1. Introduction

Unsupported molybdenum nitride with high specific surface area has attracted a great deal of interest for its excellent catalytic properties [1–5] and has the potential to replace noble metal catalysts in a number of industrial applications [6–10]. Many studies have demonstrated that molybdenum nitride is an effective and selective hydrotreating catalyst [11–13]. However, since only nitrides with high surface area are useful as efficient catalysts, an important emphasis has been placed on developing new preparation methods. There are several ways to prepare Mo nitrides of high surface area. Volpe and Boudart have developed a method for the preparation of transition metal nitrides and carbides by topotactic reaction between the relevant transition metal oxides and NH_3 [14]. In a typical

* Corresponding author. Tel.: +44-151-7943580; fax: +44-151-7943589; e-mail: yxli@liverpool.ac.uk

1381-1169/98/$19.00
PII S1381-1169(97)00237-9

process 0.2 to 1 g of precursor is employed and a passivated surface area of up to 170 m^2/g can be achieved. The properties of the resultant material appear to be strongly dependent on the synthesis conditions. Wise and Markel have reported another method for the preparation of high surface area Mo nitrides using temperature programmed reaction between MoO_3 powder and a mixture of H_2 and N_2 [15]. Their synthetic conditions were similar to those of the NH_3-based synthesis. A space velocity of 259 000 h^{-1} and a temperature ramping rate of 0.6 K/min were used for 0.5 g of MoO_3. It can, therefore, be seen that the preparation of monometallic transition metal nitrides of high specific surface area requires rather demanding conditions and the quantity of product in each batch is small, thus seriously limiting potential industrial applications [16,17]. Consequently, it is important to modify the reaction pathway in order to synthesize more material in one batch under relatively mild conditions. One possible approach for further improving the catalytic properties of Mo nitrides is to introduce a second transition metal into the nitride; this may also provide a possible way to prepare the catalysts under milder conditions. There are few reports of such research in the literature so far [18–21]. Furthermore, a thorough investigation of the surface properties, catalytic activities and bulk structure of the bimetallic nitrides obtained may lead to new insights into the chemistry of high specific area nitrides.

In this paper the bimetallic transition metal nitrides, $ZrMo_2N_x$–Mo_2N, have been synthesized, for the first time to our knowledge, by temperature programmed nitriding (TPN) Zr- and Mo-containing compounds which were prepared by impregnation or by coprecipitation. The influence of different contents of zirconium and different preparation methods on the end-catalysts are also explored. It has been found that zirconium takes the form of ZrO_2 in the end-product if the precursor is prepared by impregnation or the form of $ZrMo_2N_x$ if the precursor is prepared by coprecipitation.

2. Experimental

2.1. The synthesis of the catalysts and nomenclature

Two groups of precursors were prepared by impregnation and coprecipitation methods, respectively. For the impregnation method a given amount of MoO_3 powder was put into an aqueous solution of zirconium nitrate and the mixture was evaporated in a water-bath and then dried at 393 K for 2 h and calcined at 773 K for 3 h. For the coprecipitation method, ammonium heptamolybdate and zirconium nitrate were mixed in an aqueous solution with their ratio varied in order to make the Zr content in term of ZrO_2 (wt%) in the obtained precursor as required. The solution was evaporated in a water-bath and dried at 393 K for 2 h and calcined at 773 K for 3 h.

For the synthesis of the bimetallic end-products, 5 g of precursor was pressed into 20–40 mesh pellets and placed inside a quartz tube reactor. TPN was performed in flowing NH_3 with a space velocity of 17 000 h^{-1}. The sample was heated from room temperature to 573 K at a rate of 5 K/min and then to 973 K at 1 or 3 K/min and finally held at 973 K for another 2 h. After this the sample was rapidly cooled to room temperature in flowing NH_3 and then passivated in flowing N_2 containing a small amount of O_2 for 12 h to obtain a stable catalyst.

A pure molybdate salt, $ZrMo_2O_8$, was prepared from a mixture of aqueous solutions of zirconium nitrate and ammonium heptamolybdate with the atomic ratio of Zr:Mo = 1:2. The mixture was evaporated in a water-bath and then dried at 393 K for 2 h and calcined at 773 K for 3 h. The $ZrMo_2O_8$ obtained was also nitrided, using the same conditions, to make $ZrMo_2N_x$ with a BET surface area of 72 m^2/g. It is straightforward that the molybdate has been nitrided as the effluent consisted of H_2O, however the extent of the nitriding is unknown,

therefore an '*x*' is used to present the number of nitrogen atoms in the formula.

For the purpose of simplicity and clarity a nomenclature of the samples, both for the precursors and the end-products, is necessary. The material code takes the form of ZrMoN-*xy*, where N indicates nitride, meaning end-product after nitriding; without N indicates a precursor; *x* is a number, indicating the weight percentage of Zr in terms of ZrO_2; $y = i$ indicates the precursor prepared by impregnation and $y = c$ indicates the precursor prepared by coprecipitation. For example ZrMoN-3c is an end-product after nitriding, from the precursor prepared by coprecipitation containing 3 wt% Zr in terms of ZrO_2 and ZrMo-10i is a precursor prepared by impregnation containing 10 wt% Zr in terms of ZrO_2.

2.2. The characterization of the catalysts

2.2.1. X-ray diffraction

The passivated samples were ground gently and fixed on a backless glass slide for XRD experiments using a Rigaku Rotaflex (Ru-200B) powder X-ray diffractometer equipped with a Cu target and Ni grating monochromatic system. The working voltage of the instrument was 40 kV and the electric current was 50 mA.

2.2.2. FT-IR spectroscopy

The infrared experiments were carried out using a Bio-Rad FTS-65A Fourier transform infrared spectrometer. The sample, mixed with KBr, was ground into pellets and pressed into self-supporting discs. The resolution of the instrument was 4 cm^{-1}, the scanning range was 4000–500 cm^{-1} and the sample was located in air during the experiment.

2.2.3. Differential thermal analysis (DTA)

The differential thermal analysis of the precursors was accomplished using a DT-20B thermal analyzer (Shimadzu) employing a mixture of N_2 and NH_3 (30 ml/min, 1:1 by volume) and a heating rate of 10 K/min. 65 mg sample was used for each experiment.

2.2.4. Scanning electron microscopy (SEM)

The surface morphology of the samples was examined by using a KYKY 1000B scanning electron microscope. Before an experiment, the sample was ground in a mortar and then deposited on a circular copper slide that had been coated with a gold film. The working voltage of the machine was 20 kV and a magnification of 1000 or 3000 times was used.

2.2.5. H_2-temperature programmed desorption (TPD)

A home-made gas handling system equipped with a thermal conductivity detector (TCD) was used to perform the hydrogen temperature programmed desorption (H_2-TPD) experiments. 0.1 g of a passivated catalyst was placed in a U-shaped quartz tube and reduced in H_2 at 673 K for 2 h followed by flushing with Ar at the same temperature for 1 h. After hydrogen adsorption for 0.5 h at the required adsorption temperature in a H_2 stream with a flowing rate of 25 ml/min, the sample was cooled down to room temperature in atmospheric hydrogen and then purged with Ar to remove the physisorbed hydrogen. The measurement of H_2-TPD was carried out using Ar as the carrier gas and the heating rate was 10 K/min.

2.2.6. Evaluation of the catalytic activities

The activity measurements for cyclohexene hydrogenation (HYD), benzene hydrogenation (BHY) and thiophene hydrodesulfurization (HDS) were carried out in a medium-pressure stainless-steel system with a hydrogen pressure of 3.0 MPa. 0.5 g of catalyst in the form of 20–40 mesh pellets was loaded between pads of quartz sand plugs in a fixed-bed microreactor. Every sample was pretreated in H_2 under medium pressure (3.0 MPa) at 673 K for 2 h before the reaction run. A commercial $NiCoMo/Al_2O_3$ catalyst was sulfided in a mix-

ture of 10% H_2S/H_2 at 673 K for 2 h before the measurement. The reactant feed, consisting of 20 wt% cyclohexene, 10 wt% benzene, 1 wt% thiophene and 69 wt% cyclohexane, was introduced into the reactor by a syringe pump. The liquid hourly space velocity (LHSV) was 10 h^{-1}. The volume ratio of hydrogen to liquid was 700 and the reaction temperature was 573 K. The effluents were analyzed by gas chromatography (GC) using a 4 m long column filled with 15% carbowax (60–80 mesh particle) and a flame ionization detector (FID).

3. Results and discussion

3.1. The synthesis of the bimetallic catalysts

The synthetic conditions for the bimetallic catalysts created from precursors prepared by impregnation and their BET surface areas and pore data are listed in Table 1. Table 2 shows the synthetic conditions for the bimetallic catalysts created from precursors prepared by coprecipitation. Sample ZrMoN-3c has the highest BET surface area (132 m^2/g). As a general trend, the BET surface area of the resultant material decreases with increasing content of ZrO_2. This is exemplified clearly in Table 2, where the BET surface area drops from 118 to 69 m^2/g as the content of ZrO_2 increases from 1 to 20 wt%. It can also be seen that the synthetic conditions of catalyst ZrMoN-3c are much milder than those for pure γ-Mo_2N: the quantity in a batch was increased to 5 from 3 g; the heating rate was three times that for the monometallic Mo nitride and the space velocity of NH_3 was 17 000 h^{-1}, which is much lower than that of 37 000 h^{-1} for the synthesis of Mo_2N, thus significantly saving ammonia consumption.

3.2. The bulk structure of the precursors

Fig. 1 shows the XRD patterns of the precursors prepared by impregnation (a to e) and those

Table 1
The synthetic conditions and the surface properties of the bimetallic catalysts created from precursors prepared by impregnation

Catalyst code	ZrO_2 (wt%)	Precursor (g)	Heating rate (K/min)	NH_3 (h^{-1})	Average pore size (Å)	Pore volume (cm^3/g)	S_{BET} (m^2/g)
ZrMoN-1i	1	5	1	17 000	32.10	0.092	115
ZrMoN-3i	3	5	1	17 000	28.60	0.092	105
ZrMoN-5i	5	5	1	17 000	25.99	0.072	104
ZrMoN-10i	10	5	1	17 000	32.04	0.068	95
ZrMoN-20i	20	5	1	17 000	43.51	0.069	89
γ-Mo_2N	—	3	1	37 000	24.80	0.086	140

Table 2
The synthetic conditions and the surface properties of the bimetallic catalysts created from precursors prepared by coprecipitation

Catalyst code	ZrO_2 (wt%)	Precursor (g)	Heating rate (K/min)	NH_3 (h^{-1})	Average pore size (Å)	Pore volume (cm^3/g)	S_{BET} (m^2/g)
$ZrMo_2O_8$	—	—	—	—	69.83	0.041	25
$ZrMo_xN_y$	—	5	—	17 000	33.46	0.061	72
ZrMoN-1c	1	5	1	17 000	31.48	0.093	118
ZrMoN-3c	3	5	3	17 000	25.70	0.084	132
ZrMoN-5c	5	5	1	17 000	31.62	0.091	115
ZrMoN-10c	10	5	1	17 000	35.85	0.090	100
ZrMoN-20c	20	5	1	17 000	40.63	0.070	69
γ-Mo_2N	—	3	1	37 000	24.80	0.086	140

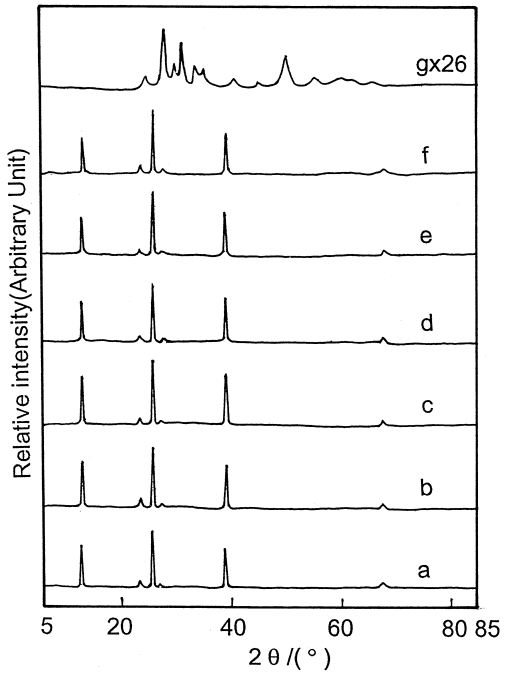

Fig. 1. XRD profiles of precursors prepared by impregnation. (a) ZrMo-1i, (b) ZrMo-3i, (c) ZrMo-5i, (d) ZrMo-10i, (e) ZrMo-20i, (f) MoO_3 and (g) ZrO_2.

for pure MoO_3 and ZrO_2 (f and g). From these profiles it is clear that the precursors with different ZrO_2 content exhibit only the diffraction peaks of MoO_3, shown in Fig. 1(f). No ZrO_2 features are visible for the MoO_3–ZrO_2 precursors. The FT-IR spectra of pure MoO_3 and the bimetallic precursors prepared by impregnation are shown in Fig. 2. Three bands at 995, 873 and 820 cm^{-1} are displayed for pure MoO_3 (Fig. 2a) which are typical stretching vibrations of Mo=O and Mo–O–Mo [22,23]. With increasing ZrO_2 content, the intensities of all three bands decrease, (Fig. 2b–f), but no new bands are detected. Our infrared experiments for pure ZrO_2 also show no IR absorption in the scanning range. Therefore, the XRD and FTIR results are consistent in showing that all the precursors contain a crystalline MoO_3 component. The XRD data, furthermore, indicate that this MoO_3 component has a preponderance of {010} planes, presumably arising from the anisotropic platelet structure favoured by pure MoO_3 [14]. The FTIR data show that the proportion of this MoO_3 component decreases significantly with increasing ZrO_2 content. The lack of signal from ZrO_2 can be attributed to the fact that both the XRD and FTIR signals from ZrO_2 are intrinsically weak making it difficult to detect this component. Another possibility for the lack of XRD signal may be that ZrO_2 is highly dispersed or in an amorphous form.

Precursors prepared by coprecipitation display rather different behaviour as shown in Fig. 3. The intensities of the diffraction peaks due to MoO_3 at 2θ values of 12.7, 25.7, 27.3 and 39.0° (Fig. 3a) gradually decrease with increasing content of Zr, while the intensity of the diffraction peak at 23.3° remains constant up to

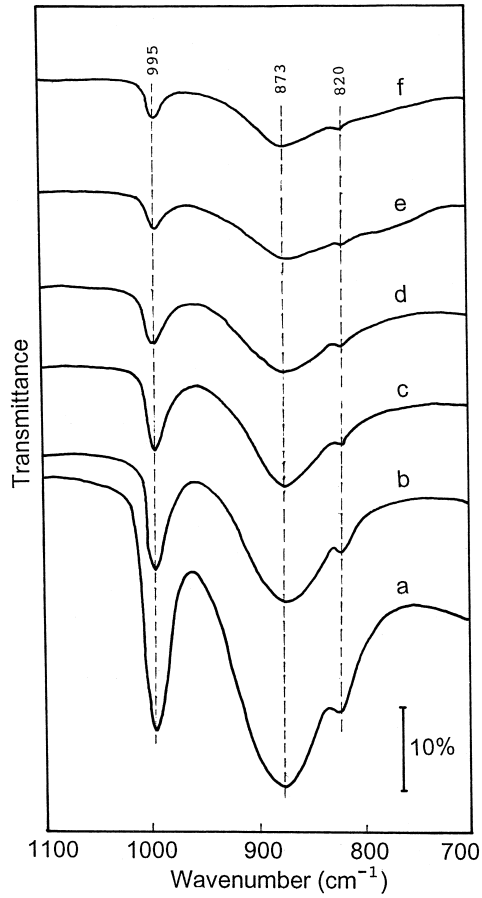

Fig. 2. FT-IR spectra of precursors prepared by impregnation. (a) MoO_3, (b) ZrMo-1i, (c) ZrMo-3i, (d) ZrMo-5i, (e) ZrMo-10i and (f) ZrMo-20i.

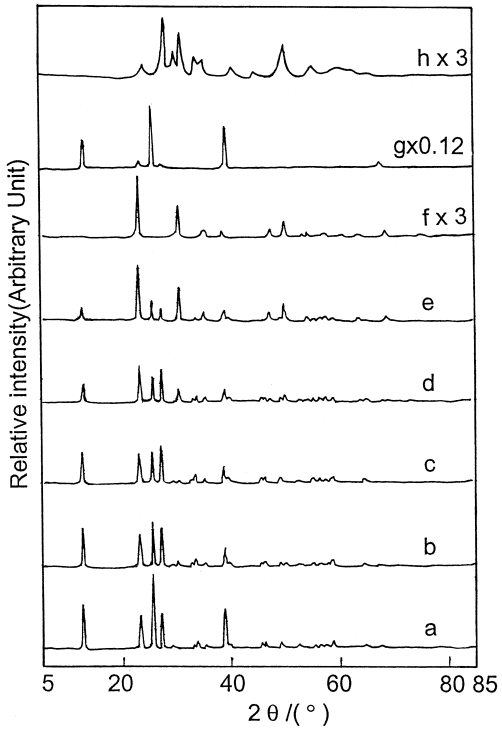

Fig. 3. XRD profiles of precursors prepared by precipitation. (a) ZrMo-1c, (b) ZrMo-3c, (c) ZrMo-5c, (d) ZrMo-10c, (e) ZrMo-20c, (f) $ZrMo_2O_8$, (g) MoO_3 and (h) ZrO_2.

10% Zr content (in terms of ZrO_2) and then increases significantly at 20% Zr content (Fig. 3b–f). Furthermore, when the Zr content reaches 10 wt%, a new diffraction peak appears with a 2θ value of 30.6° and when the Zr content reaches 20 wt%, three new diffraction peaks appear at 47.3, 49.9 and 68.8°, respectively.

The XRD profiles of the precursors in Fig. 3(a) to (e) were carefully checked and compared with each other and with those of the pure materials: $ZrMo_2O_8$ (Fig. 3f), MoO_3 (Fig. 3g) and ZrO_2 (Fig. 3h). The decrease in peak intensities at 2θ value of 12.7, 25.7 and 27.3° clearly indicates a decrease of MoO_3 content with increasing ZrO_2 content. Meanwhile, the increase of peak intensity at 2θ value of 23.3° and the appearance of peaks at 30.6, 47.3, 49.9 and 68.8° indicates the formation of $ZrMo_2O_8$. Thus, there is evidence of the coexistence of $ZrMo_2O_8$ and MoO_3 in all the precursors. Finally, as for the precursors obtained by impregnation, there are no XRD peaks from the two most intense diffractions that can unambiguously be assigned to ZrO_2 (Fig. 3h) arising from the (111) (28.57°) and ($\bar{1}11$) (31.8°) planes.

Further evidence for the formation of precursors consisting of $ZrMo_2O_8$ and MoO_3 is provided by FT-IR spectra, Fig. 4. The bands at 995, 873 and 820 cm^{-1}, arising from MoO_3, are present for all the precursors but show a decreasing trend with increasing Zr content. When Zr content (in terms of ZrO_2) reaches 10 wt%, a small band at ca. 945 cm^{-1} is observed and when the Zr content reaches 20 wt%, three new

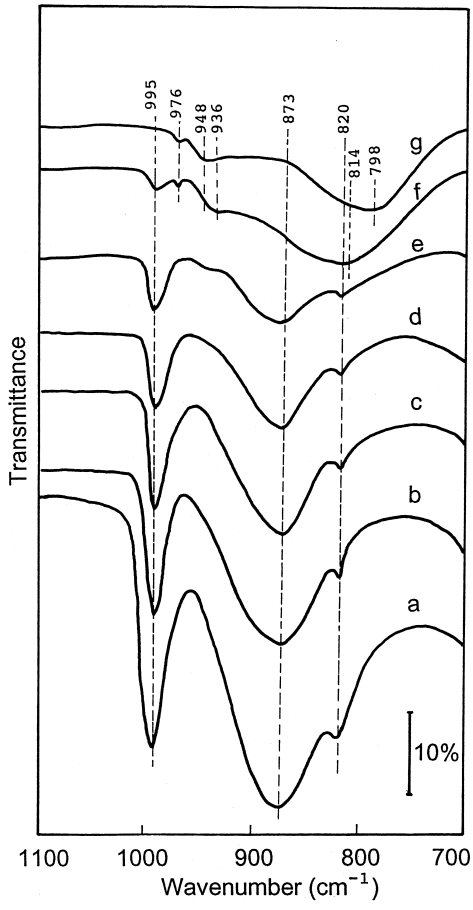

Fig. 4. FT-IR spectra of precursors prepared by precipitation. (a) MoO_3, (b) ZrMo-1c, (c) ZrMo-3c, (d) ZrMo-5c, (e) ZrMo-10c, (f) ZrMo-20c and (g) $ZrMo_2O_8$.

bands appear at 976, 936 and 814 cm^{-1} (Fig. 4f). These bands correspond closely to those of $ZrMo_2O_8$ (Fig. 4(g)).

XRD evidence also points to significant modification to the MoO_3 component upon the introduction of the second metal component. For example, there is a strong decrease in concentration of the {010} orientated planes of MoO_3 and, even at the lowest Zr content, the diffractions from the {0k0} planes of MoO_3 ($2\theta =$ 12.7°: (020); 25.7°: (040); 39.0°: (060)) decrease dramatically in intensity. Meanwhile the other diffractions of MoO_3, e.g. from the (021) plane ($2\theta = 27.3°$) and the (110) plane ($2\theta = 23.3°$), are present in greater relative intensity compared to pure MoO_3. This suggests that coprecipitation creates precursors in which the MoO_3 platelet structure, favouring the formation of {0k0} planes, is disrupted, while the creation of (021) and (110) planes is enhanced. This is reminiscent of the behaviour reported for intermediate phases formed during the reduction of MoO_3 in which crystallographic shear occurs, causing oxygen vacancies to collapse along {120} shear planes [14].

From the above results it can be concluded that different precursors are obtained by different methods of preparations: crystalline MoO_3 for the precursors prepared by impregnation and crystalline MoO_3 and crystalline $ZrMo_2O_8$ for the precursors prepared by coprecipitation. It is difficult, however, to ascertain whether amorphous and/or highly dispersed ZrO_2 is also present in either type of precursor.

3.3. The bulk structure of the bimetallic catalysts

Fig. 5 shows the XRD profiles of the bimetallic catalysts made from precursors prepared by impregnation (Fig. 5a–e) and the pure materials, γ-Mo_2N (Fig. 5f) and ZrO_2 (Fig. 5g). Only the crystalline phase of Mo_2N is detectable when the amount of ZrO_2 is 1 and 3 wt%. When ZrO_2 content is 5 wt% or more, the XRD

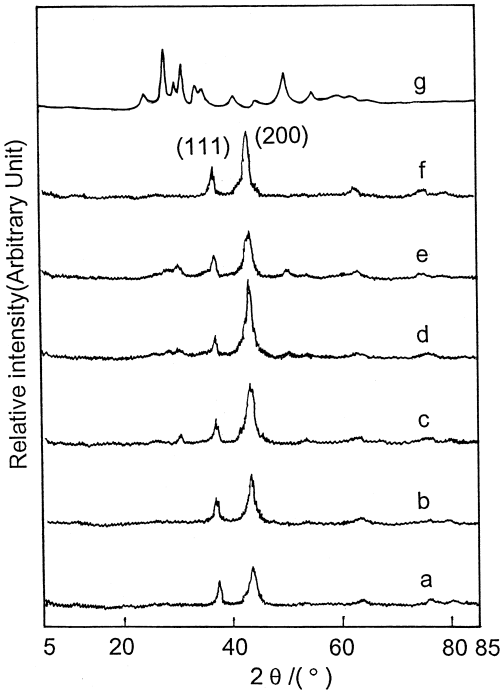

Fig. 5. XRD profiles of bimetallic catalysts obtained from precursors prepared by impregnation. (a) ZrMoN-1i, (b) ZrMoN-3i, (c) ZrMoN-5i, (d) ZrMoN-10i, (e) ZrMoN-20i, (f) γ-Mo_2N (S_{BET} = 140 m^2/g) and (g) ZrO_2.

profiles show an increasing presence of crystalline ZrO_2. It, therefore, seems that the zirconium oxide present in the precursor is not nitrided. It is relevant to note that separate TPN experiments of pure ZrO_2 also show no evidence of any nitriding occurring. We, therefore, suggest that the nitriding mechanism for the precursors follows a similar path to that of the pure MoO_3. This conclusion is supported by XRD data for the nitrided products which show that the ratio of the peak intensities from the (200) and (111) planes in Fig. 5(a)–(e) are very similar to that of high surface area pure γ-Mo_2N (f). Volpe and Boudart have previously shown that this nitriding process is a topotactic reaction in the sense that the {100} planes of Mo_2N are parallel to the {010} planes of MoO_3 [14].

Fig. 6 shows the XRD results of the bimetallic catalysts made from precursors prepared by coprecipitation (Fig. 6a–e) and those of the pure

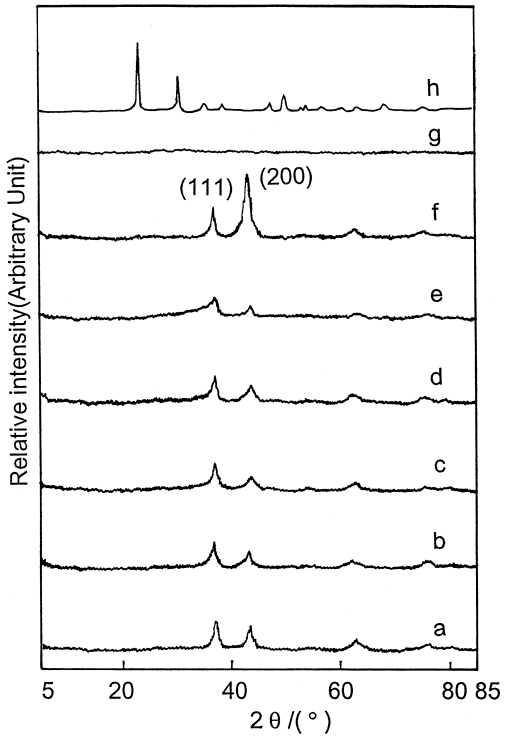

Fig. 6. XRD profiles of bimetallic catalysts obtained from precursors prepared by coprecipitation. (a) ZrMoN-1c, (b) ZrMoN-3c, (c) ZrMoN-5c, (d) ZrMoN-10c, (e) ZrMoN-20c, (f) γ-Mo_2N ($S_{BET} = 140\ m^2/g$), (g) $ZrMo_2N_x$ and (h) $ZrMo_2O_8$.

materials: γ-Mo_2N (Fig. 6f); $ZrMo_2N_x$ (Fig. 6g) and $ZrMo_2O_8$ (Fig. 6h). Only Mo_2N is detectable in the XRD data of the final resultant materials. There is no trace of the features attributable to $ZrMo_2O_8$ or ZrO_2. Separate TPN experiments on pure $ZrMo_2O_8$ show that after nitriding, all the $ZrMo_2O_8$ features (as seen in Fig. 6h) disappear to exhibit a featureless profile (Fig. 6g), which may be assigned to a bimetallic nitride, presumably $ZrMo_2N_x$. We, therefore, conclude that two kinds of nitrides are present in the end-products, Mo_2N and $ZrMo_2N_x$, in an unknown ratio.

Furthermore, Fig. 6 also shows that for each of the bimetallic nitrides, the diffraction intensity from the (200) plane of the resultant Mo_2N is much lower than that of the (111) plane. This is the opposite to what is observed with high surface area Mo_2N where the topotactic nitriding reaction leads to the (200) plane giving rise to a more intense peak than the (111) plane. Clearly, this difference arises from the fact that the MoO_3 component in the coprecipitated precursors has a different morphology in which the dominance of the {010} planes is disrupted and where (110) and (021) planes are present in significant amount. The elements of a topotactic nitriding reaction may, however, be still retained in that the loss in intensity of the Mo_2N (200) planes with increasing Zr content, seen in Fig. 6(a)–(e), parallels the loss of {0k0} planes in the original MoO_3 precursor component. However, this conclusion remains only tentative at present.

3.4. Investigation of the nitriding mechanism

Differential thermal analysis (DTA), Fig. 7, provides further information on the nitriding mechanism of the coprecipitated bimetallic precursors, carried out in a mixture of N_2 and NH_3 (1:1 by volume). Turning first to the results obtained for pure MoO_3, Fig. 7(e), an endothermic process is observed at ca. 393 K which we assign to the dehydration of the lattice water in MoO_3 on the basis of our effluent analysis during TPN. The next endothermic peak appears at around 500 K and is attributed to the transformation from Mo^{6+} to Mo^{5+} [24,25]. XRD data obtained after the third endothermic peak at ca. 653 K, indicates a mixture phase of MoO_3–MoO_2, and we, therefore, attribute this peak to a disproportionation reaction: $2Mo^{5+} = Mo^{4+} + Mo^{6+}$. XRD data obtained after the exothermic process at ca. 733 K show a pure MoO_2 phase, therefore, this peak must arise from the reduction of Mo^{6+} to Mo^{4+}. The final endothermic process observed corresponds to the nitriding reaction [5,26].

Fig. 7(b) to (d) show that all the bimetallic precursors are easier to nitride than pure MoO_3 in that the integrated area of their endothermic DTA peak for nitriding is smaller than that of MoO_3, Fig. 7(e). The detailed behaviour of each

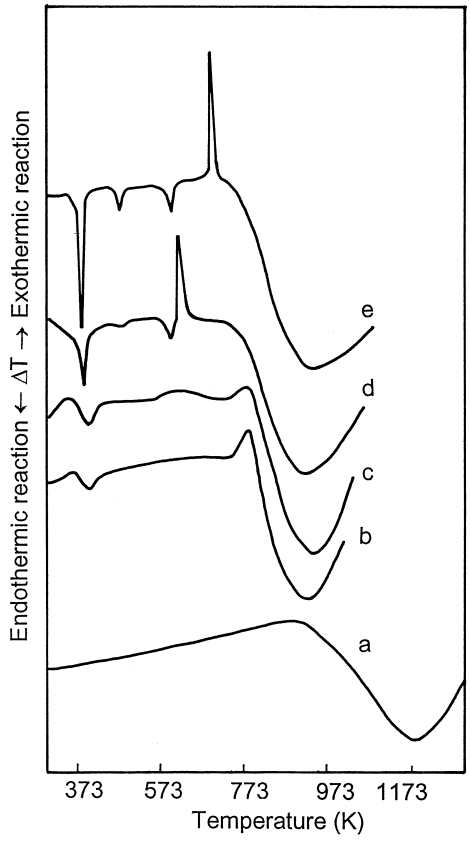

Fig. 7. Differential thermal analysis of precursors in a mixtures of N_2 and NH_3 (1:1 by volume). (a) ZrO_2, (b) $ZrMo_2O_8$, (c) ZrMo-20c, (d) ZrMo-3c and (e) MoO_3.

precursor depends strongly on Zr content. For example, the DTA profile for the precursor with 3% Zr, Fig. 7(d), is very similar to that of pure MoO_3, Fig. 7(e), except that the exothermic process to form MoO_2 takes place at a much lower temperature. This is consistent with our XRD analysis where we propose that the presence of the second metal leads to the creation of crystallographic shear planes of the type observed in intermediate phases formed during the reduction of MoO_3 to MoO_2.

The DTA profile for the ZrMo–20c precursor, Fig. 7(c), looks similar to that of $ZrMo_2O_8$, Fig. 7(b), again in accordance with XRD and FTIR data. In addition, the characteristic sharp exothermic peak of MoO_3 at 653 K disappears and is replaced by a broad hump starting at 553 K, which may indicate that the transformation of Mo^{6+} to Mo^{4+} is even easier with high ZrO_2 contents. Finally, it seems that the MoO_3 and $ZrMo_2O_8$ components of the bimetallic coprecipitated precursors are nitrided simultaneously:

$$ZrMo_2O_8 + NH_3 \overset{933\,K}{\rightarrow} ZrMo_2N_x + H_2O + N_2 \quad (1)$$

$$MoO_3 + NH_3 \overset{933\,K}{\rightarrow} Mo_2N + H_2O + N_2 \quad (2)$$

In addition, the effect of different precursors on the nitriding reaction was studied by SEM. Fig. 8(a) shows the characteristic platelet morphology of MoO_3. The morphology of the high surface area γ-Mo_2N (140 m^2/g), resulting from the topotactic reaction of MoO_3 with NH_3, is shown in Fig. 8(b) and looks very similar to that of MoO_3. This topotactic reaction brings about the crystallographic orientation relationship of $(010)_{MoO_3}//(100)_{Mo_2N}$ [14,27,28], i.e the platelets of MoO_3 which predominantly expose the (010) planes are transformed into the (100) planes of the resultant γ-Mo_2N. For such a topotactic reaction from MoO_3, the intensity of the Mo_2N (200) plane is always much higher than that of (111) planes as shown in Fig. 6. The ratio of the intensities of the (200) and (111) diffractions is considered as a quantitative parameter of texturing [14,27,28].

In contrast, the low surface area Mo nitride prepared by nitriding MoO_3 with NH_3 is doubtfully the result of a topotactic reaction [28], so the morphology of the resultant γ-Mo_2N (32 m^2/g) is expected to be different from that of the high surface area Mo nitride and hence that of MoO_3. This turns out to be the case, as exhibited in Fig. 8(c). The XRD profiles of this low surface area Mo nitride exhibits $I(111)/I(200) > 1$, the opposite of what is observed with high surface area Mo_2N.

Fig. 8(d) and (e) show the micrographs of the bimetallic material with 3 wt% of ZrO_2 prepared by impregnation, before (ZrMo-3i) and after nitriding (ZrMoN-3i). The morphologies of these two samples are similar and show the

platelet morphology exhibited by MoO_3. However, if we turn to the morphology of the 3% Zr bimetallic precursor prepared by coprecipitation, before and after nitriding, ZrMo-3c (Fig. 9f) and ZrMoN-3c (Fig. 9g), obvious differences are seen. Neither sample retains the characteristic platelet morphology of MoO_3, seen in Fig. 8(a), (b), (d) and (e). This confirms the

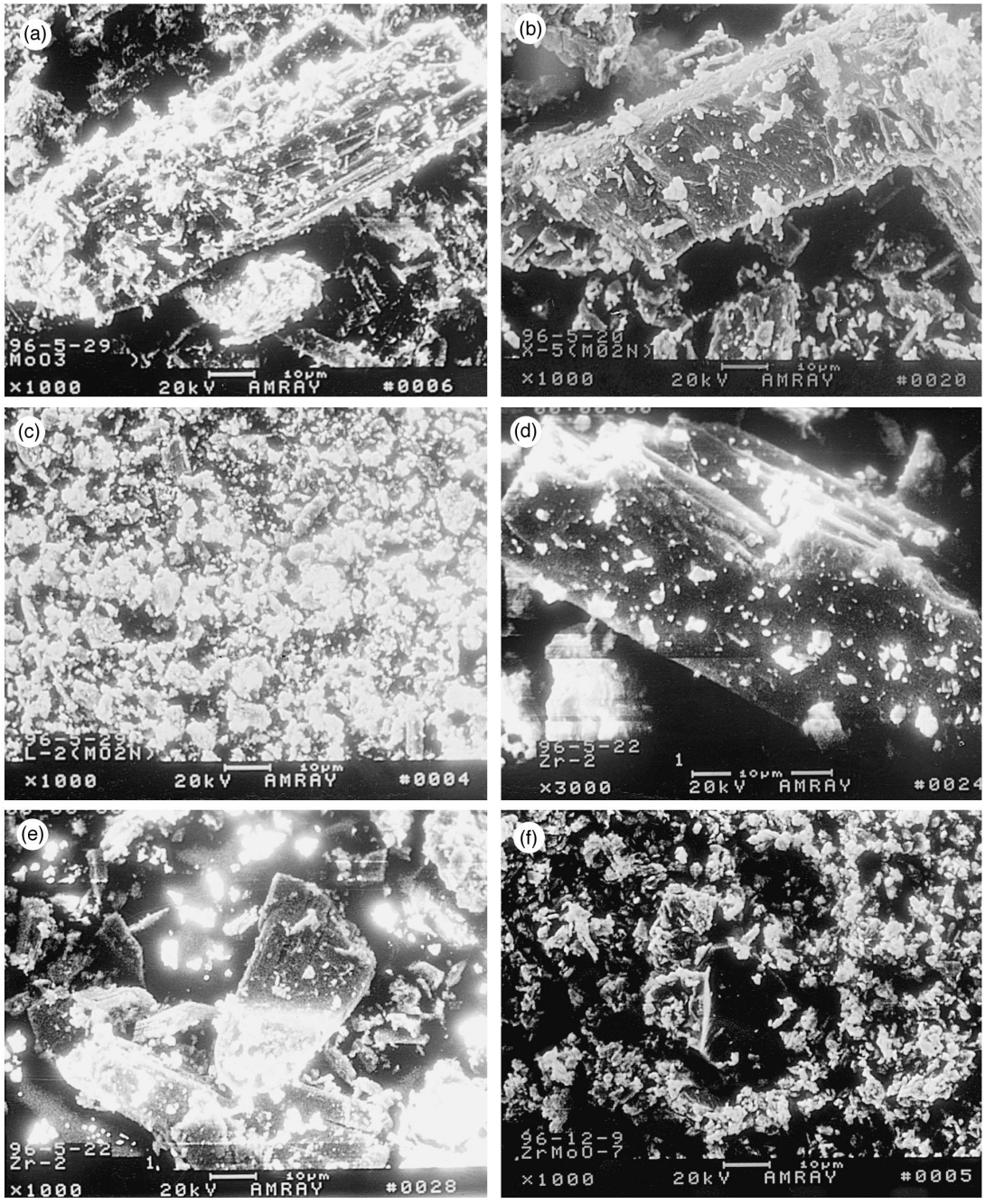

Fig. 8. Scanning electron micrographs. (a) MoO_3, (b) γ-Mo_2N ($S_{BET} = 140\ m^2/g$), (c) γ-Mo_2N ($S_{BET} = 32\ m^2/g$), (d) ZrMo-3i, (e) ZrMoN-3i ($S_{BET} = 105\ m^2/g$), (f) ZrMo-3c and (g) ZrMoN-3c ($S_{BET} = 132\ m^2/g$).

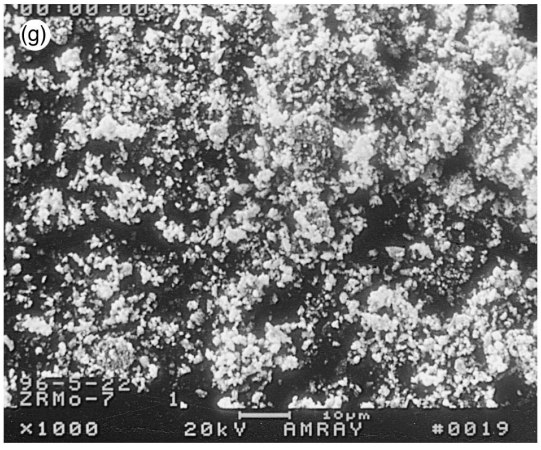

Fig. 8 (continued).

conclusions of the XRD data that the addition of the second metal component by coprecipitation destroys the platelet structure of the precursor. It is not possible, at present, to comment confidently on whether the nitridation of such precursors occurs via a topotactic reaction.

In summary, we find that the catalysts obtained after nitriding the impregnated precursors are very different from those obtained from the coprecipitation: the former consist of $ZrO_2 + Mo_2N$ and the latter contain bimetallic $ZrMo_2N_x + Mo_2N$. In particular, the impregnated catalysts undergo a topotactic nitriding reaction which retains the platelet structure of the original MoO_3 and leads to XRD patterns with $I(111)/I(200) < 1$. In contrast, coprecipitation leads to precursors in which the platelet morphology is destroyed and this is reflected in the resultant catalyst structure, where XRD show $I(111)/I(200) > 1$. Importantly, both types of catalysts are easier to nitride than pure MoO_3.

3.5. Evaluation of the catalytic activities for selective hydrogenation and hydrodesulfurization

Catalytic activity measurements for cyclohexene hydrogenation (HYD), benzene hydrogenation (BHY) and thiophene hydrodesulfurization (HDS) are shown in Fig. 9. After the catalysts had been on stream for 3 h, the catalytic properties of the bimetallic nitrides were observed to be superior to those of γ-Mo_2N and the sulfided $NiCoMo/Al_2O_3$ catalyst for conversion of cyclohexene and thiophene, while the activity of γ-Mo_2N was similar to that of the commercial hydrotreating catalyst, sulfided $NiCoMo/Al_2O_3$. However, we note that these tests were not carried out under commercial conditions and we are currently investigating the reactivity behaviour after longer on-stream times.

In the present study, the catalysts ZrMoN-1i, ZrMoN-1c and ZrMoN-3c showed the highest activities for HYD and HDS. However, the morphology and texturing of the γ-Mo_2N phase which is present in all the catalysts does not seem to play an important role in altering catalyst reactivity. For example, SEM and XRD data show that the ZrMoN-1i catalyst has a number of similarities with γ-Mo_2N, in terms of platelet morphology, Fig. 8, and extent of texturing, with both samples showing $I(111)/I(200) < 1$ (Fig. 6). Meanwhile, the ZrMoN-1c and ZrMoN-3c catalysts, with similar activities, show another type of sample morphology (Fig. 8) and their XRD data display $I(111)/I(200) > 1$. The high HYD and HDS activities of the bimetallic nitride catalysts, ZrMoN-1c and ZrMoN-3c, may be directly attributed to the presence of the bimetallic zirconium–molybdenum nitride ($ZrMo_2N_x$) phase,

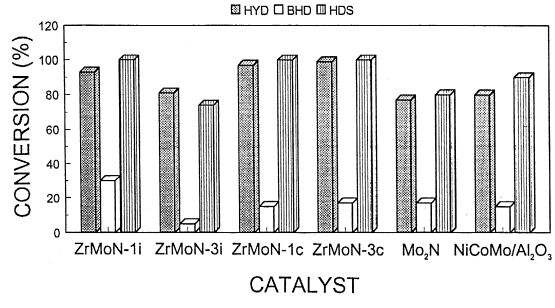

Fig. 9. Activities of hydrodesulfurization and selective hydrogenation of ZrMoN-1i, ZrMoN-3i, ZrMoN-1c, ZrMoN-3c, γ-Mo_2N (120 m^2/g) and sulfided $NiCoMo/Al_2O_3$. Reaction temperature = 573 K, LHSV = 10 h^{-1}, H_2/oil = 300 and p_{H_2} = 3.0 MPa.

however, this cannot be the case for ZrMoN-1i catalyst prepared from impregnation, where a mixture of γ-Mo_2N and ZrO_2 phases are present. It would, therefore, seem that the presence of the second metal, Zr, in itself has a promoting effect.

The improved catalytic activities of molybdenum nitrides have, in the past [29], been correlated with the ability to adsorb low temperature states of hydrogen. In order to investigate whether this is also the case for the bimetallic catalysts, we carried out hydrogen temperature programmed desorption (H_2-TPD) from the bimetallic catalysts (1–20 wt% of Zr in terms of ZrO_2) and from the precursor ZrMo-1c and pure γ-Mo_2N, after H_2 adsorption at 373 K, Fig. 10. The precursor, ZrMo-1c, does not adsorb any hydrogen as no hydrogen desorption peak appears, Fig. 10(a), while H_2 desorbs from ZrO_2 at rather high temperature (b). The hydrogen desorption from pure unsupported γ-Mo_2N occurs at 493, 645 and 773 K. It has been suggested that the H_2 desorption from Mo_2N at around 493 K is from the surface sites and that at around 773 K is from the subsurface and/or the bulk [29]. In comparison, the bimetallic nitrides display three desorption peaks which appear at lower temperatures of around 373, 523 and 753 K from Fig. 10(c) to (g), with the amount of hydrogen desorbed in the low temperature region being much greater than that in the medium and high temperature regions. This low temperature hydrogen desorption displays a sharp peak starting from as low as 310 K. In contrast, the monometallic Mo nitride does not show hydrogen desorption in this temperature region (Fig. 10h). These results obviously indicate that the existence of $ZrMo_2N_x$ can create active sites for hydrogen adsorption with lower adsorption energy, which are similar to those found with group VIII noble metals [30]. The nature of these new active sites is unknown. However, it is certainly a possibility that the improved activity of the bimetallic nitrides is linked to their extensive capacity of hydrogen adsorption.

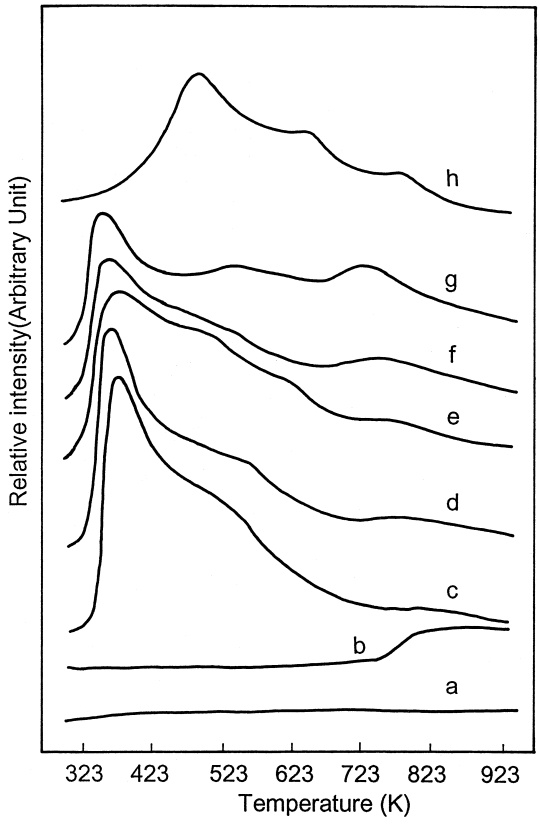

Fig. 10. H_2-TPD profiles of bimetallic catalysts after H_2 adsorption at 373 K. (a) ZrMo-1c, (b) ZrO_2, (c) ZrMoN-1c, (d) ZrMoN-3c, (e) ZrMoN-5c, (f) ZrMoN-10c, (g) ZrMoN-20c and (h) γ-Mo_2N.

4. Conclusion

An improved method has been developed for the preparation of bimetallic transition metal nitrides with high surface area by temperature programmed nitriding a material composed of $ZrMo_2O_8$ and MoO_3 with NH_3. The structures and compositions of the bimetallic catalysts produced are significantly influenced by different preparation methods of the precursors. It has been found that the end-product is composed of ZrO_2–Mo_2N if the precursor is prepared by impregnation and of $ZrMo_2N_x$–Mo_2N if the precursor was prepared by coprecipitation. XRD and SEM results reveal that after impregnation,

the bimetallic materials retain the characteristic platelet structure of MoO_3 and Mo_2N but that this structure is destroyed in the coprecipitation process. The catalytic activities of the bimetallic nitrides for HYD and HDS exceed those of the unsupported γ-Mo_2N and the commercial sulfided $NiCoMo/Al_2O_3$ catalyst, under medium pressure. The reasons for this promoting effect are, at present, open for discussion. However, H_2-TPD results indicate that the introduction of $ZrMo_2N_x$ into Mo_2N creates new active sites which adsorb hydrogen with lower adsorption energy. We, therefore, conclude that the purpose of modifying the properties of Mo_2N by introducing a second metal component has been successful in the first stage and the nitriding conditions we have used are milder than that for the preparation of Mo_2N.

Acknowledgements

The authors are grateful to the Research Institute for Petroleum Processes of the SINOPEC, the K.C. Wong Fellowships and the British Council for their valuable financial support. The authors are also grateful to Professor H. Wang of the State Key Laboratory of Catalysis and Professor E.G. Derouane of the Leverhulme Centre for useful discussions.

References

[1] S.T. Oyama, Catal. Today 15 (1992) 179.
[2] L. Volpe, M. Boudart, J. Phys. Chem. 90 (1986) 4874.
[3] J.S. Lee, L. Volpe, F.H. Riberiro, M. Boudart, J. Catal. 112 (1988) 44.
[4] G.W. Haddix, A.T. Bell, J.A. Reimer, J. Phys. Chem. 93 (1987) 5859.
[5] S.T. Oyama, J.C. Schlatter, J.E. Metcalf, J.M. Lambert, Ind. Eng. Chem. Res. 27 (1988) 1639.
[6] M. Boudart, S.T. Oyama, L. Leclercq, in: T. Seiyama, K. Tanabe (Eds.), Proc. 7th Int. Cong. Catal., Tokyo, vol. 1, Kodansha, 1980, p. 578.
[7] J.S. Lee, M.H. Yeom, K.Y. Park, I.S. Nam, J.S. Chung, Y.G. Kim, S.H. Moon, J. Catal. 128 (1991) 126.
[8] G.S. Ranhotra, A.T. Bell, J.A. Reimer, J. Catal. 108 (1987) 40.
[9] L. Leclercq, M. Provost, H. Pastor, J. Grimblot, A.M. Hardy, L. Gengembre, G. Lecleracq, J. Catal. 117 (1989) 371.
[10] R.B. Levy, M. Boudart, Science 181 (1973) 547.
[11] M. Nagai, T. Miyao, T. Tuboi, Catal. Lett. 18 (1993) 9.
[12] H. Abe, A.T. Bell, Catal. Lett. 18 (1993) 1.
[13] Y. Zhang, Z. Wei, W. Yan, P. Ying, C. Ji, X. Li, Z. Zhou, X. Sun, Q. Xin, Catal. Today 30 (1996) 135.
[14] L. Volpe, Boudart, J. Solid State Chem. 59 (1985) 332.
[15] R.S. Wise, E.J. Markel, J. Catal. 145 (1994) 344.
[16] R.S. Wise, E.J. Markel, J. Catal. 145 (1994) 335.
[17] C.H. Jaggers, J.N. Michaels, A.M. Stacy, Chem. Mater. 2 (1990) 150.
[18] P. Duwez, F. Odell, J. Electrochem. Soc. 97 (1950) 299.
[19] C.C. Yu, S. Ramanathan, F. Sherif, S.T. Oyama, J. Phys. Chem. 98 (1994) 13038.
[20] F.J. Disalvo, Science 247 (1990) 649.
[21] X. Ramanathan, C.C. Yu, S.T. Oyama, Am. Chem. Soc. Div. Fuel Chem. Prepr. 40 (1995) 998.
[22] C. Li, K. Wang, Q. Xin, X. Guo, Acta Phys. Chim. Sin. 8 (1992) 64.
[23] J.S. Chung, C.O. Bennett, J. Chem. Soc. Faraday Trans. I 82 (1986) 2155.
[24] X.S. Li, S. Sheng, H. Chen, C. Ji, Y. Zhang, Q. Xin, Acta Phys. Chim. Sin. 11 (8) (1995) 678.
[25] Y. Okamoto, A. Maezawa, T. Imanaka, J. Catal. 120 (1989) 29.
[26] S. Li, J.S. Lee, J. Catal. 162 (1996) 76.
[27] E.J. Markel, J.W. Van Zee, J. Catal. 126 (1990) 643.
[28] J.G. Choi, R.L. Curl, L.T. Thompson, J. Catal. 146 (1994) 218.
[29] J.G. Choi, J.R. Brenner, C.W. Colling, B.G. Demczyk, J.L. Dunning, L.T. Thompson, Catal. Today 15 (1992) 201.
[30] J.J.F. Scholten, A.P. Pijpers, A.M.L. Hustings, Catal. Rev. Sci. Eng. 27 (1985) 151.